Plasma Temperature in Optical Field Ionization of Gases by Intense Ultrashort Pulses of Ultraviolet Radiation

W. J. Blyth,[1] S. G. Preston,[1] A. A. Offenberger,[2] M. H. Key,[1,3] J. S. Wark,[1] Z. Najmudin,[4] A. Modena,[4] A. Djaoui,[3] and A. E. Dangor[4]

[1]*Department of Physics, Clarendon Laboratory, University of Oxford, Parks Road, Oxford OX1 3PU, United Kingdom*
[2]*Department of Electrical Engineering, University of Alberta, Edmonton, Alberta, T6G 2G7, Canada*
[3]*Rutherford Appleton Laboratory, Chilton, Didcot, Oxon, OX11 0QX, United Kingdom*
[4]*Blackett Laboratory, Imperial College, Prince Consort Road, London, SW7 2AZ United Kingdom*

(Received 9 August 1994)

Plasma electron temperatures from 3 eV to >1 keV have been measured or inferred in 10^{18} W cm^{-2} optical field ionization of helium and neon at electron densities ranging from 10^{17} to 10^{21} cm^{-3} by laser pulses of 350 fs duration and 248 nm wavelength. Increase of temperature with gas density is dominated at high densities by a combination of nonlinear inverse bremsstrahlung and stimulated Raman scattering heating which are identified as factors limiting progress to shorter extreme ultraviolet laser wavelength in recombination of optical field ionized plasmas.

PACS numbers: 52.50.Jm, 52.25.Qt, 52.25.Jm, 52.40.Nk

Theoretical studies have shown the potential of recombination in optical field ionized plasmas for extreme ultraviolet (xuv) laser action on resonance transitions of hydrogenic or lithiumlike ions [1–3]. In order to achieve shorter xuv laser wavelengths, higher intensities are required to produce ions of higher ionization potential, and the plasma density needs to be correspondingly higher to achieve high gain. The required low electron temperature (T_e) can be obtained by reducing the wavelength and the pulse duration of the field ionizing laser, but theoretical analysis suggests that heating by stimulated Raman scattering will ultimately limit the intensity and density at which the necessary low temperatures can be obtained [3]. Experimental data on temperatures of optically ionized gases are still sparse and have been obtained using significantly longer pulses and/or longer wavelengths than in the present work [4–7]. We report here the first temperature data for xuv laser relevant conditions of 350 fs pulse duration and 248 nm wavelength, similar to those in a recent experiment which showed evidence of gain in H-like lithium [8].

Spectra from Thomson scattering, stimulated Raman scattering (SRS), and ionic x-ray resonance line emission presented here give evidence of the rise of T_e with increasing plasma density (n_e). The data show that for an intensity of 10^{18} W cm^{-2} and pulse duration of 350 fs at low density ($\sim 10^{18}$ cm^{-3}), T_e is determined by above threshold ionization (ATI) and nonlinear inverse bremsstrahlung (IB) heating; while in the limit of high density ($>10^{20}$ cm^{-3}), strong IB and SRS heating impose a density and/or intensity limit for the production of cool plasma, and thus a limit on the wavelength achievable in optically ionized xuv lasers.

The experiments were performed using the Sprite KrF laser facility operating in a chirped pulse amplification mode, producing 350 fs pulses at a wavelength of 248 nm [9]. Each pulse had an energy of ~250 mJ and was focused to a 10 μm spot using a 33 cm focal length, $f/3.5$ parabolic mirror in a vacuum chamber. Low density targets ($10^{17}-10^{19}$ cm^{-3}) were provided by a static gas fill inside the chamber while high densities ($10^{19}-10^{21}$ cm^{-3}) were achieved with a high pressure solenoid-valve gas jet with a 1 mm diameter cylindrical nozzle [10]. Two gases were used—He to provide a plasma with a uniform ionization profile and Ne as an example of a higher Z material relevant to xuv lasers.

Thomson scattering and SRS sidescatter of the incident laser light were recorded at 150° and 90° to the incident laser direction using $f/5$ achromat lenses which imaged (with 10× magnification) the scattered light onto 200 μm wide slits of two 0.3 m Czerny-Turner spectrometers. The spectrometer slits on the 90° detection channel were oriented parallel to the laser axis so that the scattering was spatially resolved with 40 μm resolution in the axial direction, but integrated in the radial direction since the radial extent of the plasma was smaller than the ~40 μm spatial resolution. The slits on the 150° spectrometer were oriented perpendicular to the laser axis, so that scattering was integrated over a 40 μm axial length, as well as integrated radially. Streak cameras were used as detectors in order to discriminate the weak Thomson signal from delayed stray light.

SRS backscattered light was collected by the parabolic focusing mirror, and 8% of this was split off using a 0.6 mm thick quartz pellicle and focused onto the photocathode of a streak camera. In order to discriminate against stray light, a glass filter was used with a cutoff at 300 nm. SRS backscatter could therefore only be measured at high densities, where the wavelength shift was high enough to be above the cutoff. The streak camera was calibrated to measure the absolute level of SRS reflectivity. An x-ray minispectrometer with a TlAP crystal was used to measure

 0031-9007/95/74(4)/554(4)$06.00

the x-ray spectrum in the region of 5–15 Å. The x rays passed through a 10 μm Be filter and were recorded on Kodak DEF x-ray film.

The results are divided into two parts. For low density static fill targets, Thomson scattering was measured, and this was used to infer electron temperatures. At intermediate gas jet densities ($10^{19}-10^{20}$ cm^{-3}), Thomson scattered signals were obscured by plasma self-emission light, so that temperatures could not be deduced. At high gas jet densities ($>10^{20}$ cm^{-3}) in Ne, scattered signals were again recorded due to the high level of SRS sidescatter in both the 90° and 150° channels when the laser energy was high. These signals coincided with several other phenomena including SRS backscatter and x-ray spectra from Ne^{9+}, which indicated the onset of SRS heating. We first discuss the low density data, then the high density data.

At low electron densities ($n_e = 3 \times 10^{17}$ to 3×10^{19} cm^{-3}) the laser pulse length (350 fs) is shorter than the electron-electron collision time (~1–5 ps), so there is not time for the plasma to thermalize. Moreover, the ATI distributions for electrons from different ionization stages vary, so there is not a well defined single electron temperature in the plasma. It is not possible, therefore, to fit the data with theoretical Thomson scattering spectra using single Maxwellian velocity distributions.

Typical Thomson scattered spectra are shown in Fig. 1 for He static gas fills. At the lowest densities, Thomson scattering is in the incoherent regime, where the width of the spectrum is determined by Doppler broadening due to thermal motion of the electrons. For these data, we can infer average temperatures by fitting Gaussian curves (see Fig. 2).

For static fill densities above 10^{18} cm^{-3}, this approach can no longer be used, since collective scattering becomes important. Here, the spectra depart in three ways from the form of Thomson scattering for a thermal plasma. First, the electron density deduced using the normal Thomson scattering theory is inconsistent with that deduced from the known density of He atoms. Second, the spectra are not symmetrical, showing more scattering on the redshifted than on the blueshifted side (see Fig. 1) which might indicate the onset of SRS. Third, the amount of scattering due to the "zero-damped" ion resonance [7] is not consistent with the form of the rest of the spectrum. If the electrons are in thermal equilibrium, the fraction of light scattered at low frequency shifts (into the central "ion feature" of the spectrum) is maximized when $T_e/T_i \gg 1$ and is determined by the value of $\alpha = (k\lambda_D)^{-1}$, where k is the wave number of the plasma waves and λ_D is the Debye length. The value of α also determines the shape of the spectrum at high frequency shifts (the outer "electron feature" of the spectrum). In our data, the fraction scattered in the ion feature is higher than predicted from the value of α deduced from the shape of the electron feature. It is therefore assumed that fitting normal Thomson scattering spectra (i.e., spectra calculated using single Maxwellian velocity distributions) to these data is not valid.

The approach used in this work is to assume that although the plasma is nonthermal, the Bohm-Gross dispersion relation can still be used to determine the frequency of electron-plasma waves, and that the peaks seen in the redshifted data are due to scattering from these waves. For He we know the density of atoms, so for full ionization, n_e and T_e can be deduced (see Fig. 2). In Ne, the spatially averaged scattering signal comes from a mixture of ionization stages so the density is not well defined. This prevents us from deducing accurate temperatures for Ne at these intermediate densities.

High density data are now presented which suggest that SRS becomes strong enough in the limit of high laser energy and density to cause additional heating. Direct

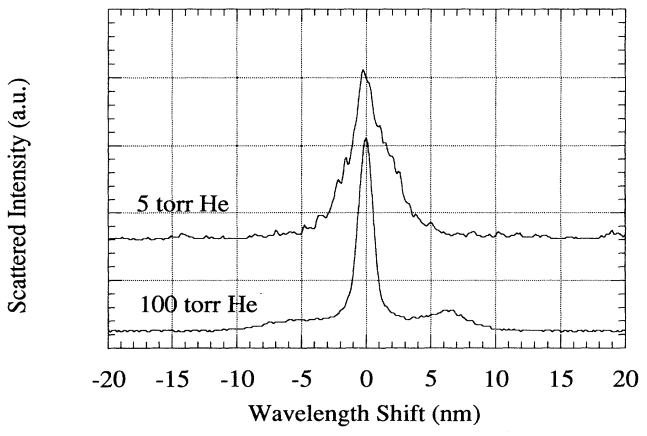

FIG. 1. Thomson scattered spectra for helium at *atomic* densities of 1.7×10^{17} cm^{-3} (5 Torr) and 3.3×10^{18} cm^{-3} (100 Torr).

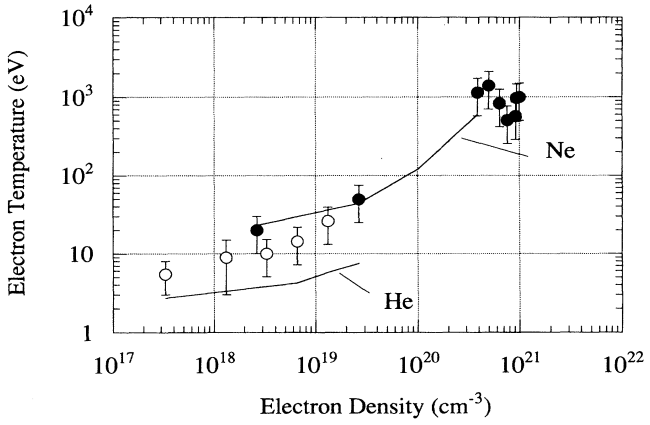

FIG. 2. Experimental temperatures are shown for neon (closed circles) and helium (open circles). The simulated temperatures for the experimental conditions (300 fs pulse) are shown as solid lines; temperatures at the peak of the pulse are shown for helium, and temperatures at the end of the pulse are shown for neon.

evidence of this comes from the SRS backscatter and SRS sidescatter measurements. Figure 3 shows the typical variation in SRS backscatter reflectivity observed as a function of the laser energy for $n_e \sim (5-8) \times 10^{20}$ cm^{-3} produced with the Ne gas jet. The highest energies correspond to the maximum laser energy that could be delivered to target. Lower energy was obtained by attenuating the beam by factors of 1.5 and 3; shot-to-shot variations in laser energy and focal spot uniformity (factor of 2 variations measured with a far-field monitor) account for the scattered distribution. Since the focal spot distribution is not uniform, the SRS reflectivity and concomitant heating will vary.

There is a rapid onset of the SRS instability as the laser energy increases, with reflectivities exceeding 2% in Ne (and 5% in He) at the highest energies. The high levels of SRS backscatter coincided with the onset of SRS sidescatter measured in the 90° and 150° channels. The measured SRS reflectivity can be used to infer the fraction of laser energy that goes into plasma waves, which is of the order of 1 mJ for Ne. If we assume for a simple energy balance calculation that this energy is equally divided between the electrons in the focal region of the plasma (10 μm diameter and 100 μm length) and thermalized, then for $n_e = (5-8) \times 10^{20}$ cm^{-3} the inferred heating would be $\sim 0.8-1.2$ keV. Consequently, the combined IB and SRS heating should result in >1 keV electron temperatures. Such values are consistent with the 90° and 150° SRS sidescatter data. If it is assumed that scattering measured on both channels comes from the same region of plasma, then the difference between the wavelength shifts for the two angles can be used to deduce temperature and density via the Bohm-Gross relation. This analysis gives $n_e = (5-8) \times 10^{20}$ cm^{-3}, and $T_e = 1-2$ keV, depending on laser intensity and the driving pressure in the Ne gas jet.

An independent confirmation of these temperatures is provided by the x-ray spectra, measured by integrating over ten shots. Spectra were only observed when the laser energy was greater than 160 mJ (i.e., intensities $> 6 \times 10^{17}$ W cm^{-2}), suggesting they are connected to the high SRS levels. Figure 4 shows an x-ray spectrum from a Ne gas jet target. The resonance lines and the recombination continuum of He-like Ne together with the resonance lines of H-like Ne are clearly visible. The unusual feature of the higher intensity of He-γ compared to He-β with its apparent indication of population inversion can be explained by opacity of He-β [11].

Ionization to Ne^{9+} could occur in two ways. Optical field ionization (OFI) would require an intensity over 4×10^{19} W cm^{-2}, which could only be achieved through self-focusing of the laser to a channel less than 1.5 μm in diameter. 1D modeling with the hydrocode MEDUSA shows that even if this occurred in a channel of 1 mm length (the diameter of the gas jet), subsequent recombination would give an emitted x-ray photon number less than 1% of that observed experimentally. We therefore discount this mechanism.

An alternative process is collisional ionization to Ne^{9+}. In order to investigate this, simulations were performed with the 1D hydrocode MEDUSA to calculate the x-ray yield from an initial 10 μm diameter 100 μm long vocal volume in which we assumed deposition of energy by SRS heating and thermalization of the electron energies. The x-ray yield was calculated for IB heating only and compared to that predicted for combined IB and SRS heating. For 2% SRS reflectivity, implying a temperature rise during the pulse to >1 keV, transient ionization to Ne^{9+} is calculated to give a much greater yield of x-ray photons in the measured spectral lines ($>5\times$), consistent with experimental observations. We therefore associate the x-ray yield in Fig. 4 with additional heating accompanying high level SRS.

Finally, in Fig. 2, we show MEDUSA simulations of the temperatures expected from ATI and IB heating alone, with heat loss from the focal region included. The total energy was 250 mJ in a 350 fs FWHM Gaussian pulse and 10 μm FWHM Gaussian spatial profile, with a peak

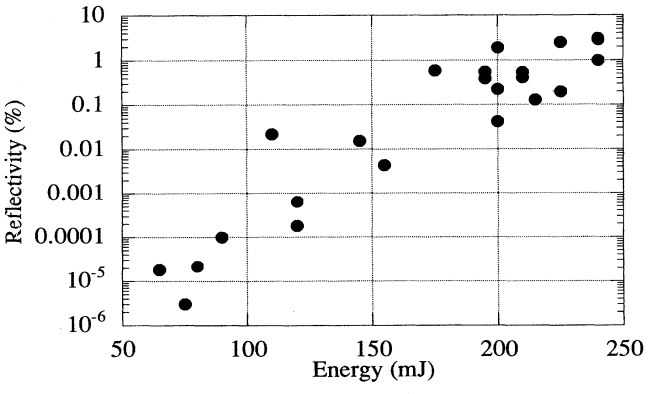

FIG. 3. Stimulated Raman scattering reflectivity as a function of laser energy for an electron density of $(5-8) \times 10^{20}$ cm^{-3} in neon.

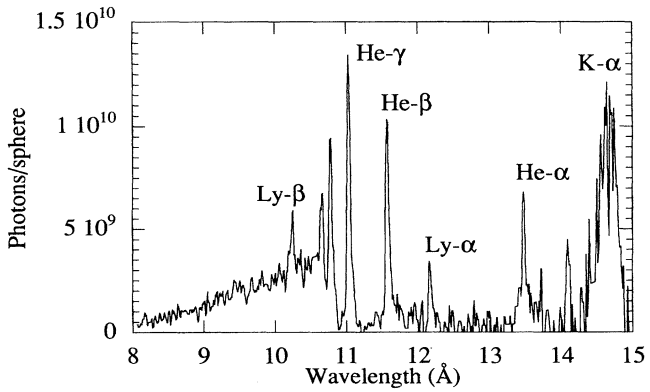

FIG. 4. K-shell x-ray spectrum in neon for laser intensity of 10^{18} W cm^{-2}.

intensity of 10^{18} W cm^{-2}, corresponding to the conditions of the experiments. For the static fill targets (He and low pressure Ne) the temperatures are deduced from Thomson scattering signals averaged over the pulse which should correspond to T_e at about the peak of the pulse. The simulation temperatures shown for these densities are those at the peak of the pulse so that comparison can be made with the experiment.

At electron densities below 3×10^{19} W cm^{-3} in the simulations, the temperature is principally determined by ATI and IB heating. The error bars for the experimental data at these densities denote the temperature according to whether a Gaussian fit (giving an upper bound) or a Bohm-Gross fit (giving a lower bound) is used. The measured T_e is therefore qualitatively consistent with the simulations at these densities for He and quantitatively for Ne. However, above 2×10^{18} cm^{-3} in He (where T_e is deduced from a Bohm-Gross fit), the temperature increases faster with density than is predicted by the simulations. This could have two causes. First, SRS heating could be responsible. We could not measure SRS backscatter directly for low density because the wavelength shift was not above the cutoff of the filter. However, the asymmetry of the Thomson scattering at 90° and 150° could indicate the onset of SRS sidescatter, which would suggest the SRS backscatter may be playing a role. The second possible cause may be that the IB heating rate is higher than predicted by MEDUSA. Recent calculations by Polishchuk and Meyer-ter-Vehn [12] give a modified Coulomb logarithm that increases the IB heating rate above the more usual form discussed by Schlessinger and Wright [13].

For high density Ne, the temperature is deduced from a comparison between the 90° and 150° SRS sidescatter. To compare experiment with the simulations, we show for Ne the maximum simulated temperatures that are reached. These occur towards the end of the pulse, since IB continues to heat the plasma until the laser has passed. The temperature at the end of the pulse is also more relevant to xuv lasers since this is when recombination and subsequent gain would occur. When SRS heating, corresponding to 2% reflectivity, is included, the calculated temperature is approximately doubled. This is within the error bars shown in Fig. 2.

We now consider the implications of these results for potential xuv lasers. Simulations by Eder *et al.* [3] show that to achieve high gain and efficiency in Li-like Ne, the electron temperature needs to be ~40 eV for an electron density of 5×10^{20} cm^{-3}, and for OFI production of the ions, the intensity should be 3×10^{17} W cm^{-2}. Our data in Fig. 2 show $T_e > 1$ keV for $n_e = 5 \times 10^{20}$ cm^{-3} and 350 fs, 10^{18} W cm^{-2} pulses. However, for the parameters of Eder's calculations, our experimental intensity and pulse duration would both be reduced by a factor of 3. Since the SRS gain coefficient scales as $I^{1/2}t$ and must exceed about 20 for significant SRS, extrapolation of our experimental conditions suggests that the instability should be suppressed for the conditions of Eder *et al.* Indeed, as observed experimentally, the SRS reflectivity is found to decrease 4 orders of magnitude for an intensity reduction of 3.

It also follows that increasing Z beyond Ne would require increased density along with intensity scaling as approximately Z^6 which implies that the SRS instability will rapidly recur for higher Z. OFI recombination lasers on Li-like ions will therefore be restricted to atomic numbers <12, and thus to wavelengths longer than about 6 nm.

In conclusion, the electron temperature of plasmas produced by optical field ionization in a regime relevant to recombination x-ray lasers has been measured for the first time. At low densities, the temperature is dominated by ATI and IB heating. At the highest densities [$(5-8) \times 10^{20}$ cm^{-3}] and laser intensity (10^{18} W cm^{-2}), we conclude from experiment and calculation (SRS backscatter and sidescatter, x-ray yield, and electron heating) that SRS is responsible for strong plasma heating ($T_e > 1$ keV). This puts a limit on the intensity that can be used to create a "cold" plasma for recombination lasers, and thereby puts a lower limit on the x-ray laser wavelength that can be produced.

[1] N. H. Burnett and P. B. Corkum, J. Opt. Soc. Am. B **6**, 1195 (1989).
[2] N. H. Burnett and G. D. Enright, IEEE J. Quantum Electron. **26**, 1797 (1990).
[3] D. C. Eder, P. Amendt, and S. C. Wilks, Phys. Rev. A **45**, 6761 (1992).
[4] R. R. Freeman, P. H. Bucksbaum, H. Milchberg, S. Darack, D. Schumacher, and M. E. Geusic, Phys. Rev. Lett. **59**, 1092 (1987).
[5] W. P. Leemans, C. E. Clayton, W. B. Mori, K. A. Marsh, A. Dyson, and C. Joshi, Phys. Rev. Lett. **68**, 321 (1992).
[6] T. E. Glover, T. D. Donnelly, E. A. Lipman, A. Sullivan, and R. W. Falcone, Phys. Rev. Lett. **73**, 78 (1994).
[7] A. A. Offenberger, W. Blyth, A. E. Dangor, A. Djaoui, M. H. Key, Z. Najmudin, and J. S. Wark, Phys. Rev. Lett. **71**, 3983 (1993).
[8] Y. Nagata, K. Midorikawa, S. Kubodera, M. Obara, H. Tashiro, and K. Toyoda, Phys. Rev. Lett. **71**, 3774 (1993).
[9] I. N. Ross, A. R. Damerell, E. J. Divall, J. Evans, G. J. Hirst, C. J. Hooker, J. R. Houliston, M. H. Key, J. M. D. Lister, K. Osvay, and M. J. Shaw, Opt. Commun. **109**, 288 (1994).
[10] Y. Li and R. Fedosejevs, J. Phys. E (to be published).
[11] Analysis of this spectrum is being prepared for publication.
[12] A. Y. Polishchuk and J. Meyer-ter-Vehn, Phys. Rev. E **49**, 663 (1994).
[13] L. Schlessinger and J. Wright, Phys. Rev. A **20**, 1934 (1979).